Received: 17 November 2021 | Revised: 24 February 2022 | Accepted: 15 March 2022

IET Generation, Transmission & Distribution

DOI: 10.1049/gtd2.12465

The Institution of Engineering and Technology WILEY

ORIGINAL RESEARCH

Performance analysis of three-phase five-leg transformers under DC bias using a new frequency-dependent reluctance-based model

Sevket Canturk[1] | **Murat Erhan Balci**[1] | **Mehmet Hakan Hocaoglu**[2] | **Ahmet Kerem Koseoglu**[3]

[1]Department of Electrical and Electronics Engineering, Balikesir University, Balikesir, Turkey

[2]Department of Electrical and Electronics Engineering, Istanbul Commerce University, Istanbul, Turkey

[3]BEST Transformer Co., Balıkesir, Turkey

Correspondence
Sevket Canturk, Department of Electrical and Electronics Engineering, Balikesir University, Balikesir 10145, Turkey.
Email: scanturk@balikesir.edu.tr

Abstract

This paper presents a reluctance-based model considering the frequency-dependent loss nature of the windings for the analysis of three-phase five-leg transformers under grid voltages with direct current (DC) bias. This is very important especially for proper determination of their harmonic current distortion and maximum loading capability (MLC) under DC-biased grid voltage conditions. To figure out the developed model's validity under sinusoidal and DC-biased grid voltage cases, it is comparatively analyzed with the model based on 2D finite element method (FEM). Thus, for the considered transformer type operated under DC bias, the excitation current's harmonic pollution, losses, and reactive power demand parameters are analyzed by using the developed model. Additionally, by regarding these performance parameters, the DC susceptibilities of the considered-type transformer and the single-phase shell-type transformer are comparatively evaluated. Finally, for the studied grid voltage conditions, the effects of two important design considerations as (i) magnetic core material selection and (ii) legs' cross-sectional area sizing on the MLC are investigated. It is concluded from these investigations that under saturation conditions, the transformers, which have the core material with higher permeability or lower reluctance, draw higher excitation current, and have lower MLC ratio when compared to ones having the core material with lower permeability or higher reluctance. However, for unsaturated transformers, which work under DC bias, the case is the opposite to that in saturation conditions. On the other hand, under DC bias conditions, the effect of cross-sectional area sizing on the MLC ratio is much more for the transformer with high permeable magnetic core material with regards to ones with low permeable magnetic core material.

1 | INTRODUCTION

The direct current (DC) or quasi DC current flowing through transformers, which are AC machines traditionally designed for rated AC voltage, current, and power conditions at supply grid frequency, is generally called transformer DC-biased case in the literature [1, 2]. In the AC power networks, DC-biased cases can occur due to induction of very low-frequency voltages on transmission lines related to variation of the geomagnetic field and improper design of grounding systems of high voltage DC transmission systems and photovoltaic distributed generation units [3–7]. Transformers can be saturated with DC bias. Thus, they may have significant increase in losses, reactive power demands, and current harmonic pollution [7–11]. The maximum loading capabilities of the DC-biased transformers are significantly reduced due to their overheating that is related to the extremely increased losses [7, 12, 13].

As a result, it can clearly be mentioned that under DC or quasi DC-biased conditions, analysis of the transformers behaviour and their proper design are essential to provide safe operation of the power system. In the literature, for these analysis and design studies, finite element method (FEM)-based transformer models are generally simulated [14, 15]. However, FEM-based models require long computation time and resources. For this reason, reluctance-based models of the transformers have been preferred in recent studies due to their computational efficiency.

On the other side, it can be mentioned from the literature that the frequency dependence of transformer winding resistances is neglected in reluctance-based transformer models [16–18] except the model of shell-type single-phase transformers recently proposed by the authors [7]. Additionally, in [7], three different approaches based on (i) rated primary side current, (ii) rated total loss, and (iii) rated primary side winding loss are considered for calculating the maximum loading capability (MLC) of transformers under the voltages with DC bias. It also points out that the third approach should be taken into account for safe operation of the transformers for the respected voltage conditions. Here, it should be underlined that the frequency dependence of the windings resistors should be regarded to obtain much more accurate results on loss determination and sizing of the transformers for non-sinusoidal conditions.

In this study, firstly, a reluctance-based model is proposed for three-phase five-limb core-type transformers by regarding the frequency dependence of the windings in Matlab/SIMULINK software. Secondly, to show the developed model's validity under sinusoidal and DC-biased grid voltage cases, it is comparatively analyzed with the FEM model, which is one of the most preferred techniques for transformer analysis and design in the literature [19]. Here, it should be mentioned that the FEM modelling technique is also widely employed for the analysis of transformers under DC-biased voltage and non-linear loading conditions [20–22]. And then, for the considered-type transformer operated under DC bias, behaviour of the losses, excitation current's harmonic distortion, and reactive power demand are investigated with using the developed model. Additionally, by regarding these performance parameters, the DC susceptibilities of the considered-type transformer and the single-phase shell-type transformer are comparatively evaluated. Finally, for the same conditions, the effects of two main design considerations as (i) magnetic core material selection and (ii) legs' cross sections on the MLC are parametrically analyzed.

2 | DEVELOPED MODEL

As mentioned before, reluctance-based transformer models do not regard the windings losses' frequency-dependent nature except the recent one which is presented for shell-type single-phase transformers by the authors [7]. The model developed here is an extension of the reluctance-based model [7] to three-phase five-limb transformers.

The schematic of the model constituted in Matlab/SIMULINK software is presented in Figure 1. The electrical and magnetic equivalent circuit parts of the model are interpreted as follows.

2.1 | The developed model's electrical equivalent circuit

By regarding the frequency-dependent nature of the windings losses [7, 23, 24], for phase m (a, b, and c), there are below-mentioned circuit components in the model's electrical equivalent circuit part

- R_{pmDC} and R_{smDC} are DC resistances of the primary and secondary windings, respectively,
- $v_{pmEC}(t)$ and $v_{smEC}(t)$ are controlled voltage sources which represent the frequency-dependent winding resistances related with P_{EC} ($R_{ECpmh} = h^2 R_{ECpm1}$ and $R_{ECsmh} = h^2 R_{ECsm1}$) for the primary and secondary sides, respectively,
- $v_{pmOSL}(t)$ and $v_{smOSL}(t)$ are controlled voltage sources which represent the frequency-dependent winding resistances related with P_{OSL} ($R_{OSLpmh} = h^{0.8} R_{OSLpm1}$ and $R_{OSLsmh} = h^{0.8} R_{OSLsm1}$) for the primary and secondary sides, respectively,
- $R_{\mathrm{Mp_m}}$ and R_{Msm} denote the parts of the resistance related with the core loss shared to the primary and secondary sides, respectively.

The connection between the electric and magnetic equivalent circuits is provided by the converter block in Figure 2, which is available in the Matlab/SIMULINK library. They act as a conversion between the electric and magnetic quantities according to Equation (1) [25]:

$$\begin{bmatrix} F_{xm}(t) \\ e_{xm}(t) \end{bmatrix} = \begin{bmatrix} N_{xm} & 0 \\ 0 & N_{xm} \times \frac{d}{dt} \end{bmatrix} \begin{bmatrix} i_{cxm}(t) \\ \Phi_{xm}(t) \end{bmatrix} \quad \text{for } x = p,\ s \text{ and } m = a,\ b,\ c \tag{1}$$

where for phase $m = a$, b, and c at the primary and secondary sides ($x = p$, s), $e_{x_m}(t)$, and $i_{cx_m}(t)$ stand for the instantaneous values of the induced voltages and excitation currents. N_{x_m} denotes the winding turns number, $F_{x_m}(t)$ is the magnetomotive force and $\Phi_{x_m}(t)$ is the total magnetic flux at phase m ($m = a$, b, and c) of the primary and secondary sides ($x = p$, s), respectively.

In order to find the currents and voltages in the electrical circuit, the transient analysis in Matlab/SIMULINK can be achieved with using the differential state equations expressed in Equations (2) and (3) for phase $m = a$, b, c

$$v_{\mathrm{pm}}(t) = R_{\mathrm{pmDC}} i_{\mathrm{p_m}}(t) + v_{\mathrm{pmEC}}(t) + v_{\mathrm{pmOSL}}(t) + N_{\mathrm{pm}} \frac{d\Phi_{\mathrm{pm}}}{dt} \tag{2}$$

$$v_{\mathrm{sm}}(t) = R_{\mathrm{smDC}} i_{\mathrm{sm}}(t) + v_{\mathrm{smEC}}(t) + v_{\mathrm{smOSL}}(t) + N_{\mathrm{sm}} \frac{d\Phi_{\mathrm{sm}}}{dt} \tag{3}$$

where $i_{\mathrm{pm}}(t)$ and $i_{\mathrm{sm}}(t)$ can be expressed as

$$i_{\mathrm{pm}}(t) = \frac{e_{\mathrm{pm}}(t)}{R_{\mathrm{Mpm}}} + i_{\mathrm{Cpm}}(t) \tag{4}$$

$$i_{\mathrm{sm}}(t) = \frac{e_{\mathrm{sm}}(t)}{R_{Msm}} + i_{\mathrm{Csm}}(t) \tag{5}$$

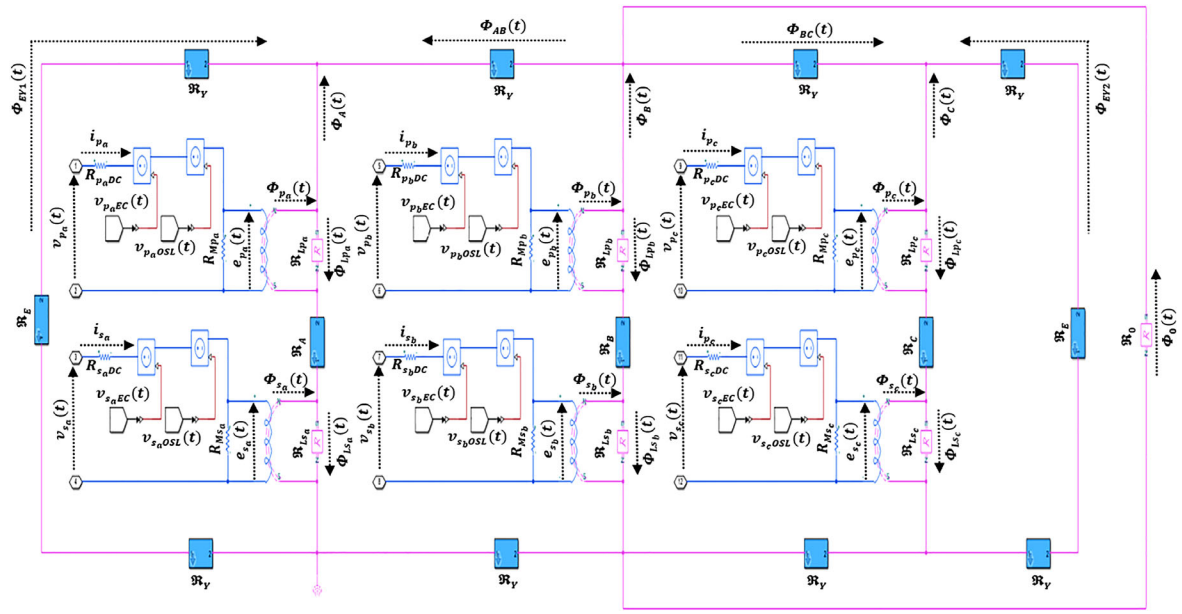

FIGURE 1 Circuit diagram of the model developed for three-phase five-leg transformers

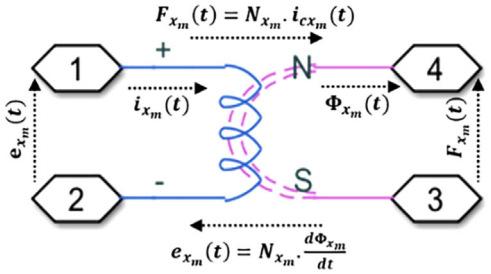

FIGURE 2 The converter block employed in the developed model

and $v_{\mathrm{pmEC}}(t)$, $v_{\mathrm{smEC}}(t)$, $v_{\mathrm{pmOSL}}(t)$ and $v_{\mathrm{smOSL}}(t)$ are defined as follows:

$$v_{\mathrm{pmEC}}(t) = \sum_{h=1}^{h\max} \sqrt{2} I_{\mathrm{pmh}} \sin(h\omega_0 t + \varphi_{\mathrm{pmh}}) R_{\mathrm{ECpm1}} h^2 \quad (6)$$

$$v_{\mathrm{smEC}}(t) = \sum_{h=1}^{h\max} \sqrt{2} I_{\mathrm{smh}} \sin(h\omega_0 t + \varphi_{\mathrm{smh}}) R_{\mathrm{ECsm1}} h^2 \quad (7)$$

$$v_{\mathrm{pmOSL}}(t) = \sum_{h=1}^{h\max} \sqrt{2} I_{\mathrm{pmh}} \sin(h\omega_0 t + \varphi_{\mathrm{pmh}}) R_{\mathrm{OSLpm1}} h^{0.8} \quad (8)$$

$$v_{\mathrm{smOSL}}(t) = \sum_{h=1}^{h\max} \sqrt{2} I_{\mathrm{smh}} \sin(h\omega_0 t + \varphi_{\mathrm{smh}}) R_{\mathrm{OSLsm1}} h^{0.8} \quad (9)$$

2.2 | The developed model's magnetic circuit

The magnetic equivalent circuit part needs the core geometry data of the transformer and the *B–H* curve of the core material so that the saturation effect is taken into account in the model. For the studied transformer, these required data are obtained from the transformer manufacturer, and they are given in the appendixes.

The magnetic equivalent circuit consists of 13 reluctance blocks: three main limbs '$\mathfrak{R}_{\mathrm{A}}$, $\mathfrak{R}_{\mathrm{B}}$, $\mathfrak{R}_{\mathrm{C}}$', two outer limbs '$\mathfrak{R}_{\mathrm{E}}$' and eight yoke '$\mathfrak{R}_{\mathrm{Y}}$' reluctance blocks. Other blocks in the circuit can be expressed as

- $\mathfrak{R}_{Lp_m}$ and $\mathfrak{R}_{Ls_m}$ represent the reluctance of the air gap in which the primary and secondary windings leakage flux flows for phase *m*, respectively,
- $\mathfrak{R}_0$ is the leakage flux flowing from core to tank that can be obtained by the no-load tests.

$\mathfrak{R}_{Lp_m}$ and $\mathfrak{R}_{Ls_m}$ can be expressed in terms of inductance ($L_{C\varkappa_m}$) and turn number ($N_{\varkappa_m}$) of the respected winding as

$$\mathfrak{R}_{L\varkappa} = {N_{\varkappa m}}^2 / L_{\varkappa m} \; for \; \varkappa = p, \; s \; sides \; and \; m = a, b, c \; \text{phases} \quad (10)$$

For the iterative calculation of the magneto-motive forces ($F_{\mathrm{A}}(t)$, $F_{\mathrm{B}}(t)$, $F_{\mathrm{C}}(t)$, $F_{\mathrm{E}}(t)$ and $F_{\mathrm{Y}}(t)$) dropped on the $\mathfrak{R}_{\mathrm{A}}$, $\mathfrak{R}_{\mathrm{B}}$, $\mathfrak{R}_{\mathrm{C}}$, $\mathfrak{R}_{\mathrm{E}}$ and $\mathfrak{R}_{\mathrm{Y}}$ reluctances, the calculation block shown in Figure 3 is used. During the calculation, firstly, the magnetic fluxes (Φ) of the main legs, outer legs, and yokes, which flow through the respected reluctance blocks in the magnetic equivalent circuit model, are measured, and they are divided by their cross-sectional area. Hence, the magnetic flux density values (B) of the core parts are found.

Then, with the 'Lookup Table' block, the magnetic field strength values (H) are calculated according to the *B–H* characteristic curve of the core material entered in the parameters section. As a result of multiplying H with the length of the legs or

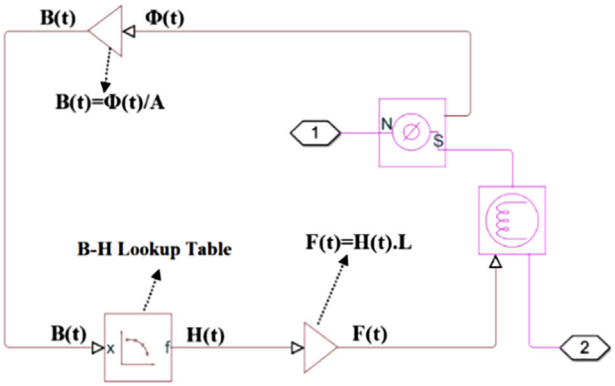

FIGURE 3 Modelling of $\mathfrak{R}_A$, $\mathfrak{R}_B$, $\mathfrak{R}_C$, $\mathfrak{R}_E$, $\mathfrak{R}_Y$ reluctance blocks

yoke (l), the magneto-motor forces on these parts are found. In the model simulation, the equations presented in (2– 5) and the expressions of the magnetic fluxes given in (11–15) are solved simultaneously in the time domain

$$\Phi_{EY1}(t) + \Phi_A(t) + \Phi_{AB}(t) = 0 \tag{11}$$

$$\Phi_{AB}(t) + \Phi_{BC}(t) = \Phi_B(t) + \Phi_0(t) \tag{12}$$

$$\Phi_{EY2}(t) + \Phi_C(t) + \Phi_{BC}(t) = 0 \tag{13}$$

$$\Phi_{xm}(t) = \Phi_m(t) + \Phi_{Lxm}(t) \tag{14}$$

$$\Phi_{Lxm}(t) = \frac{F_{xm}(t)}{\mathfrak{R}_{Lxm}} \tag{15}$$

In Equations (11–15), $\Phi_m(t)$ stands for the fluxes flowing through main limbs of the core, $\Phi_{Lxm}(t)$ are the leakage fluxes flowing through $\mathfrak{R}_{Lxm}$, and $\Phi_0(t)$ is the leakage flux flowing through $\mathfrak{R}_0$.

3 | SIMULATION RESULTS

In this section, firstly, for the rated pure sinusoidal voltage and the rated sinusoidal voltage with DC bias, the results of the 2D FEM model created in Maxwell/Ansys software and the reluctance-based model developed in Matlab/Simulink software are comparatively analyzed by regarding no-loading and loading cases of the transformer. Thus, it is aimed to show the validity of the computationally efficient reluctance model for DC excitation conditions. Secondly, under the rated sinusoidal voltage with several DC-biased levels, behaviour of the losses, reactive power demand, excitation current's harmonic distortion and MLC are investigated with using the developed model. Finally, for DC-biased conditions, the effects of two main design considerations as (i) magnetic core material selection and (ii) legs' cross sections on the losses and MLC are investigated. The schematic of the test system set-up for the performed analyses is given in Figure 4. The DC voltage value (V_{DC}) dropped on the energy transmission line in the system is provided by DC voltage sources. With respect to the DC voltage drop values on the transmission line per kilometre mentioned in [26, 27], V_{DC} is increased up to 10 V/km in the simulations. The transformer modelled in the test system has rated values as 70 MVA, 50 Hz, and 154/34.5 kV. The transmission line has a length of 100 km and a voltage level of 154 kV. Other parameters of the energy transmission line and the modelled transformer can be found in the appendix. The transformer is loaded with a pure resistor in the simulations. Accordingly, the fundamental frequency

reactive power [28], which is demanded by the transformer, can be calculated with using Equation (16):

$$Q_1 = \sum_{m=a,b,c} V_{pm1} I_{pm1} \sin\theta_{pm1} \tag{16}$$

where V_{pm1} and I_{pm1} denote voltage and current rms values at the primary side of phase m for supply frequency, and θ_{pm1} is difference between their phase angles.

Total demand distortion index of the transformer primer current at m phase ($TDDI_{pm}$) is calculated as

$$TDDI_{pm}(\%) = 100\frac{\sqrt{\sum_{h=2}^{h\max} I_{Pmh}^2}}{I_{PR}} \tag{17}$$

where I_{PR} is the rated primary side current of the transformer.

3.1 | Validity analysis of the developed model

In validation tests, the preferred transformer type is simulated by 2D FEM analysis in ANSYS Maxwell software [29]. The transformer geometry including the windings and the core created in this software is presented in Figure 5, which shows the flux density distribution in the core when V_{DC} is 10 V/km. On the other hand, ANSYS Maxwell's circuit editor tool is used for the transformer's supply voltage and loading. For the accuracy of the simulation, the transient analysis is preferred where the mesh number is 10,000 and the eddy current losses are not neglected. M5-0.30 mm is preferred as the core material and the B–H and P–B curves of this material, which should be entered in ANSYS Maxwell, are presented in the appendix. Thus, the reduced waveforms of currents and voltages to pu obtained from the simulations of 2D FEM and the developed models in the supply cases with sinusoidal and DC voltages are given in Figures 6–9.

In these figures, it is seen that the instantaneous current and voltage waveforms obtained from the simulations performed with both models are quite similar. Additionally, for the pure sinusoidal (V_{DC} = 0 V/km and I_{PDC} = 0 pu) and the DC bias (V_{DC} = 10 V/km and I_{PDC} = 0.45 pu) conditions, the root mean square difference (RMSD) between the voltage and current waveforms obtained with the FEM and developed models is presented in Table 1. From this table, it can be concluded that both models give very close results to each other.

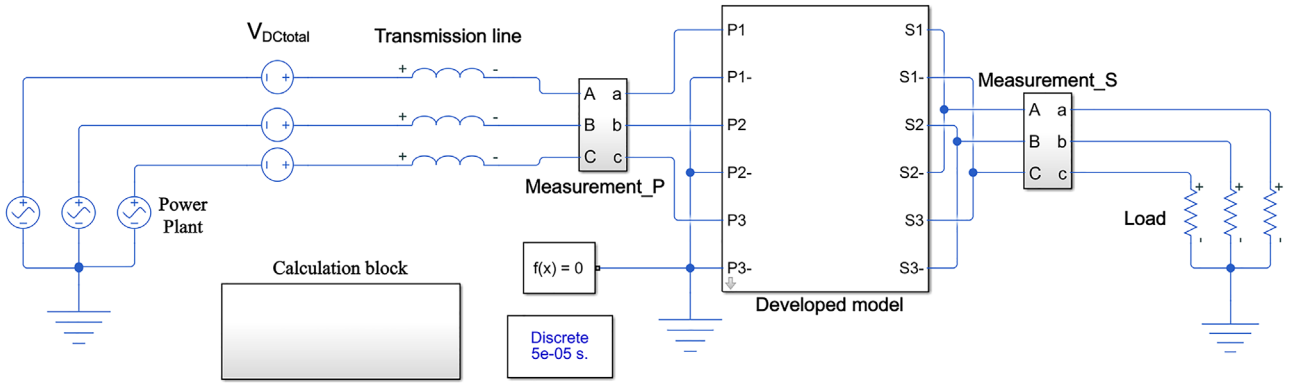

FIGURE 4 Test system created in Matlab/SIMULINK software

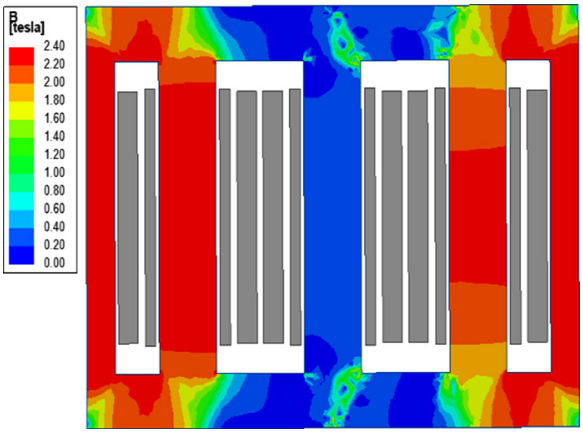

FIGURE 5 2D geometry of the studied three-phase five-limb power transformer

TABLE 1 RMSE values for both models

	50% loading		No-load	
V_{DC} (V/km)	**0.0**	**10.0**	**0.0**	**10.0**
I_{PDC} (pu)	**0.0**	**0.45**	**0.0**	**0.45**
I_{pa} (pu)	0.00241	0.00642	–	0.01895
I_{pa} (pu)	0.00252	0.00815	-	0.01256
I_{pa} (pu)	0.00245	0.00918	–	0.01487
V_{sa} (pu)	–	5.93×10^{-4}	–	–
V_{sa} (pu)	–	6.78×10^{-4}	–	–
V_{sc} (pu)	–	6.45×10^{-4}	–	–

3.2 | Analysis of the studied transformer's behaviour for DC-biased grid voltage

In this section, for the transformer operated under grid voltage with various DC-biased levels, (i) the harmonic spectrum, total demand distortion, and rms values of the primary winding currents, (ii) DC, eddy current, other stray, no-load, and total losses, and (iii) reactive power demand quantities are analyzed with the developed model. In the examination, the transformer is unloaded and the DC-biased value is increased from 0 to 10 V/km.

Under no-loading condition, for the simulated V_{DC} levels, the rms primary side phase currents (I_{pa}, I_{pb}, and I_{pc}) in pu

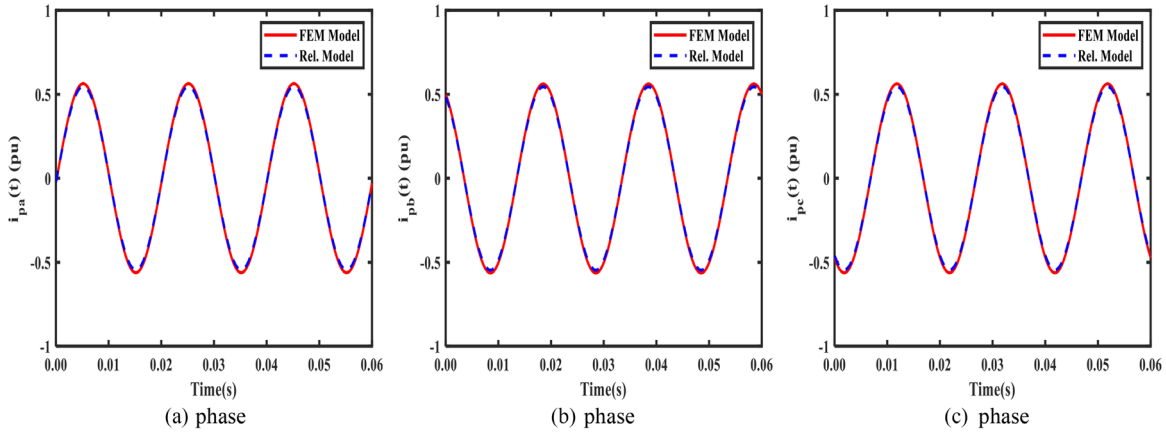

FIGURE 6 Waveshapes of primary side currents obtained with FEM and the developed models under low (40%) loading and sinusoidal condition ($V_{DC} = 0$ V/km)

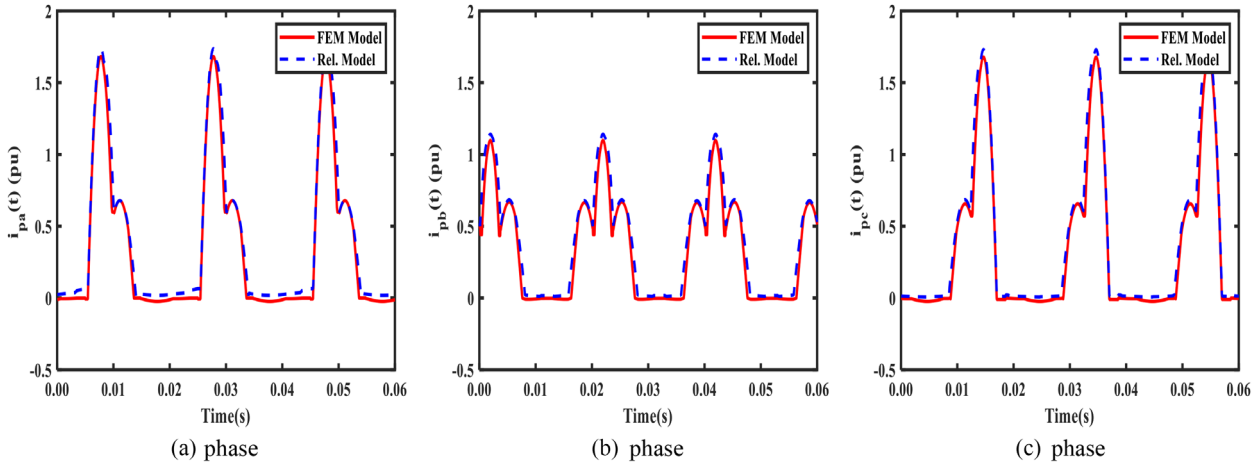

FIGURE 7 Waveshapes of primary side currents obtained with FEM and the developed models under no loading and DC-biased condition (V_{DC} = 10 V/km)

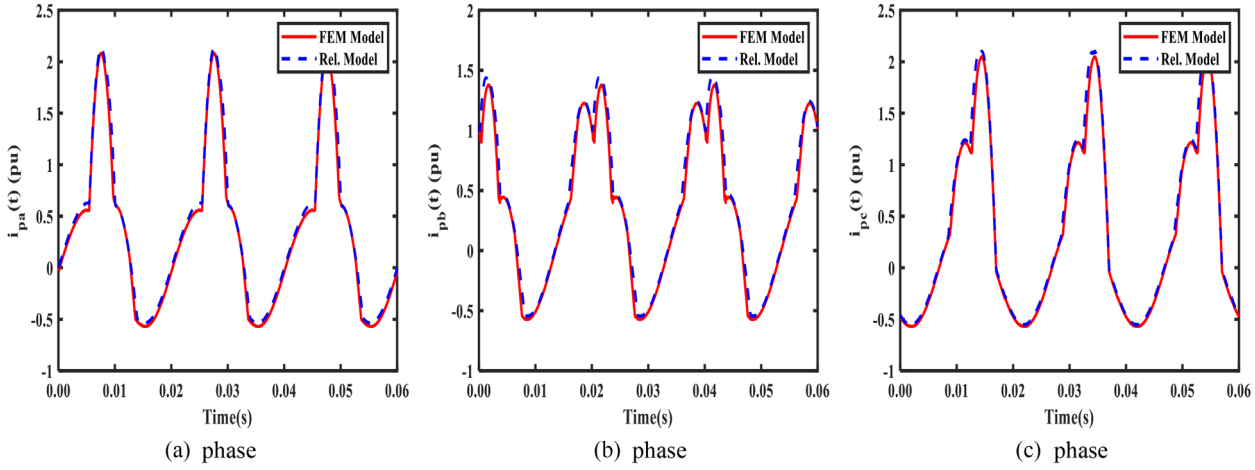

FIGURE 8 Waveshapes of primary side currents obtained with FEM and the developed models under low (40%) loading and DC-biased condition (V_{DC} = 10 V/km)

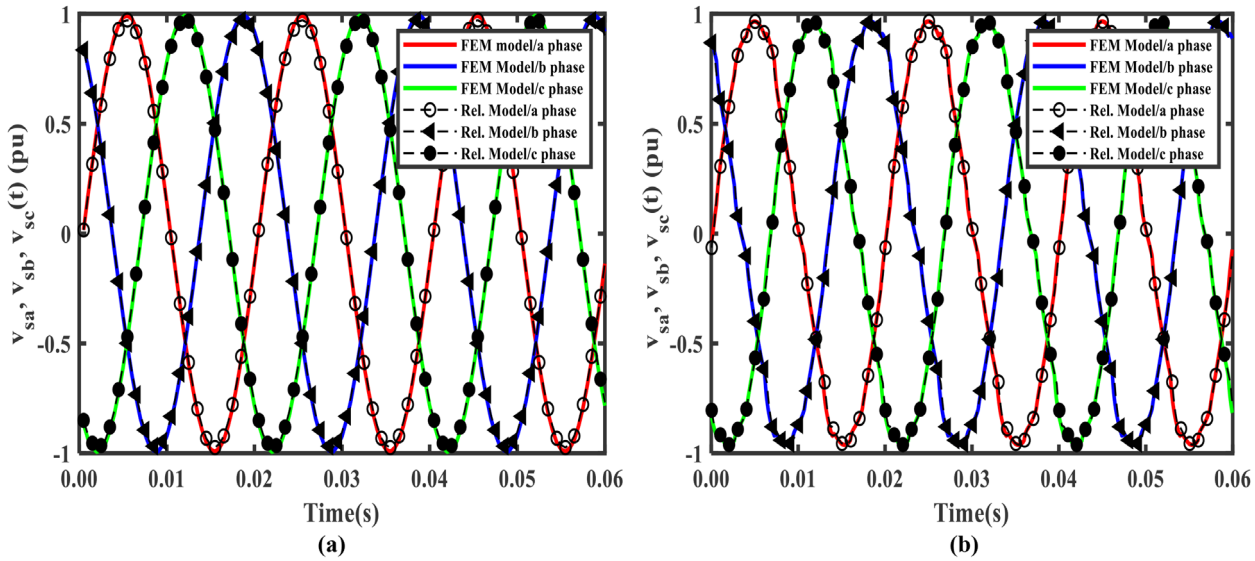

FIGURE 9 Waveshapes of secondary sides terminal voltages for 40% loading of the transformer under (a) sinusoidal (V_{DC} = 0 V/km) and (b) DC-biased grid voltage condition (V_{DC} = 10 V/km)

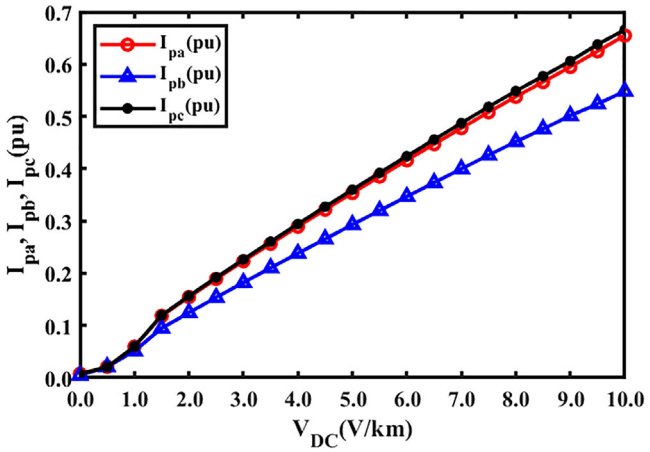

FIGURE 10 The variation of I_{Pa}, I_{Pb}, and I_{Pc} with V_{DC}

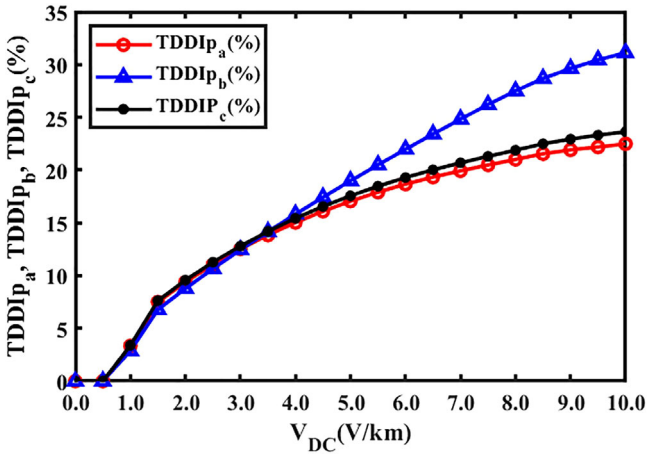

FIGURE 11 The variation of $TDDI_{Pa}$, $TDDI_{Pb}$, and $TDDI_{Pc}$ with V_{DC}

and their total demand distortion values ($TDDI_{pa}$, $TDDI_{pb}$, $TDDI_{pc}$) are plotted in Figures 10 and 11. Figure 10 shows that in the considered V_{DC} interval, I_{pa}, I_{pb}, and I_{pc} increase from 0.03 pu to 0.65, 0.54, 0.66 pu, respectively. The DC and harmonic components of the primary side phase currents (I_{PmDC} and I_{Phm} for $m = a, b, c$) in pu are shown in Figure 12.

It can be pointed out from Figures 11 and 12 that V_{DC} results in excessive increment of no-load phase currents harmonic distortion. For 10 V/km of V_{DC}, $TDDI_{pa}$, $TDDI_{pb}$, and $TDDI_{pc}$ are 21%, 32%, and 22%, respectively. All three figures also show that there is an unbalance among primary side phase currents at fundamental and non-fundamental frequencies due to the asymmetrical construction of transformer core.

The normalized values (N) of P_{DC}, P_{EC}, P_{OSL}, P_{TL}, P_{NL}, and Q_1 are given in Figure 13. Note that in this figure, to provide the normalized values, the losses (P_{DC}, P_{EC}, P_{OSL}, P_{TL}, P_{NL}) are divided by the rated total loss of the transformer and the fundamental harmonic reactive power (Q_1) is divided by the rated power of the transformer. Similar to findings for single-phase shell-type transformer presented in [7], it can be pointed out that P_{DC}, P_{TL}, and Q_1 significantly increase with V_{DC} level. The

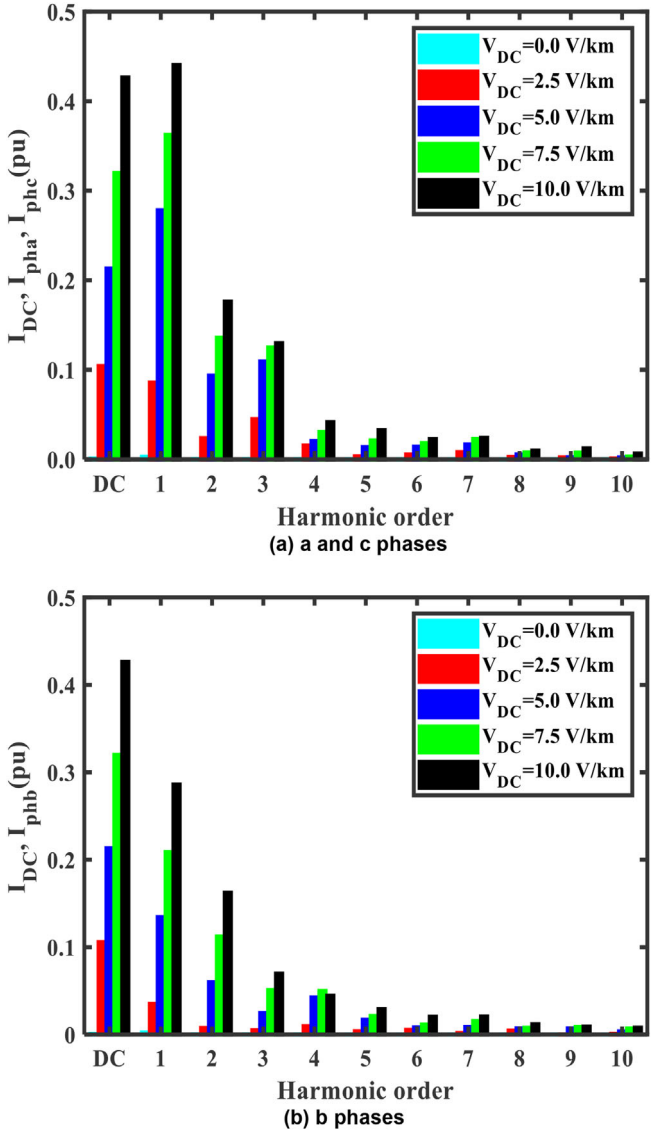

FIGURE 12 The harmonic spectrums of the primary side current for the simulated V_{DC} levels

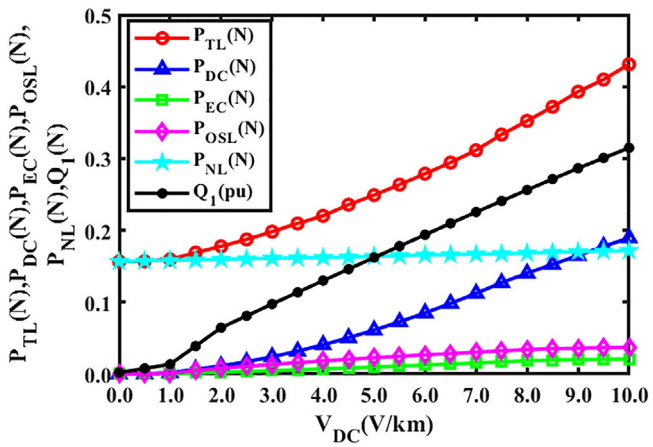

FIGURE 13 The variation of the losses and fundamental harmonic reactive power demand with V_{DC}

TABLE 2 Excitation current rms and demand distortion values, power losses, and reactive power demand for single-phase shell-type and three-phase five-leg transformers

	Single-phase shell-type		Three-phase five-leg	
V_{DC} (V/km)	0	10	0	10
I_p (pu)	0.017	0.889	0.018	0.592
TDDIp (%)	0.955	44.05	0.521	24.66
P_{DC} (N)	0.98×10^{-4}	0.321	0.87×10^{-4}	0.193
P_{EC} (N)	1.14×10^{-4}	0.084	1.02×10^{-4}	0.046
P_{OSL} (N)	1.71×10^{-4}	0.042	1.57×10^{-4}	0.035
P_{NL} (N)	0.221	0.268	0.166	0.182
Q_1 (N)	0.012	0.517	0.014	0.325

increment of DC-biased level leads to an increase in P_{DC} higher than P_{EC} and P_{OSL}.

In addition to that, for the single-phase shell-type and three-phase five-leg transformers modelled in [7] and this study, respectively, under sinusoidal voltage ($V_{DC} = 0$ V/km) and the highest DC-biased voltage condition ($V_{DC} = 10$ V/km), I_p, $TDDI_p$, P_{DC}, P_{EC}, P_{OSL}, P_{NL}, and Q_1 values are given in Table 2. Note that I_p and TDDIp values for the studied three-phase five-leg transformer are mean values of those quantities measured at phases, and both transformers have the same voltage and frequency ratings and the same X/R ratio of the windings, three-phase five-leg transformer has the power rating three times of single-phase one. From this table, it can be mentioned that when compared with the three-phase five-leg transformer, all these quantities of single-phase shell-type one increase much more with DC bias. In other words, the studied three-phase transformer type is much more immune to the DC-biased voltages.

3.3 | Effect of the transformer's major core design parameters on the MLC under DC bias

In this section, for DC-biased conditions, the effects of two main design considerations as (i) magnetic core material selection and (ii) legs' cross sections on the MLC are investigated.

For this aim, under DC-biased voltage, MLC or derating factor of three-phase five-leg transformer is analyzed by using the developed model. MLC in percentage can be found as the ratio of the highest permissible load apparent power (S_M) and the rated power of the transformer (S_{TR}):

$$\text{MLC}\,(\%) = 100\frac{S_M}{S_{TR}} \tag{18}$$

For safe operation of the transformer under the grid voltage with DC bias, the highest permissible load apparent power is obtained as the supplied load apparent power in which the loss of the primary winding equals the rated loss of primary winding [7].

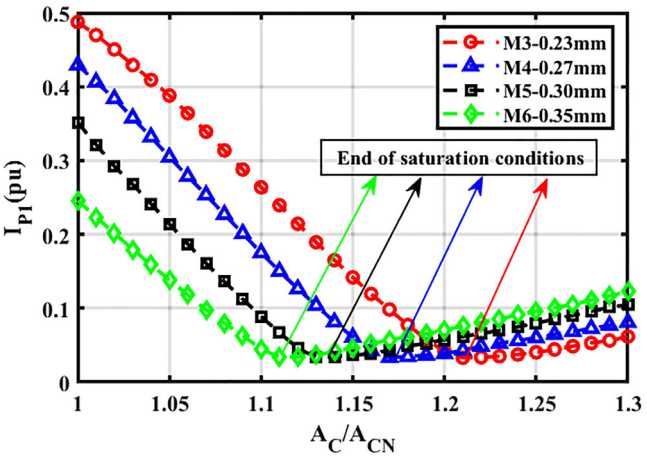

FIGURE 14 Variation of I_{P1} with increment of core cross-sectional area for different core materials under 10 V/km DC bias

Accordingly, in the analysis, the variation of MLC is investigated for different core materials under DC bias. For the analysis, the considered core materials are in order of magnetic permeability from the largest to the smallest as follows M3-0.23 mm, M4-0.27 mm, M5-0.30 mm, and M6-0.35 mm. For each material, the *B–H* curves and the core loss resistances are entered to the model. Core dimensions and winding impedances are kept constant during the analyses. This means that the core produced from material with high magnetic permeability will have a smaller reluctance. In addition to the different core material selections, the cross-sectional areas of the yokes and outer legs of the transformer are varied in the analysis. The cross-sectional areas are not changed on the main legs where the windings are located. This is because the cross-section increase in the main legs changes the size and impedance of the windings.

With the increment of core cross-section area up to 30%, under no-load condition the variations of the fundamental frequency current rms (I_{P1}) values of the three-phase five-leg transformers, which have different core materials as M3-0.23 mm, M4-0.27 mm, M5-0.30 mm, and M6-0.35 mm are given in Figure 14. For the analysis, the DC-biased level is simulated as 10 V/km in the system. In the figure, the cross-sectional area increment is denoted as the ratio of the core cross-sectional area (A_C) and nominal core cross-sectional area (A_{CN}).

It is seen from Figure 14 that for all four magnetic core materials, with the increment of A_C/A_{CN} ratio, at the first I_{P1} decreases and attains its lowest value, and then it increases. Thus, it can clearly be mentioned that for the interval of A_C/A_{CN} ratio in which I_{P1} decreases, the transformer is under saturation. On the other hand, for the rest interval of A_C/A_{CN} ratio in which I_{P1} increases, the studied transformer has low magnetic flux density (B) values below the knee point of *B–H* curve of the core material, and it needs high excitation current.

In addition, it can also be pointed out from Figure 14 that for M3-0.23 mm, M4-0.27 mm, M5-0.30 mm, and M6-0.35 mm materials, the saturation of the transformer is eliminated where A_C/A_{CN} is about 1.21, 1.17, 1.14, and 1.12, respectively. Under saturation conditions, the transformer with the core material

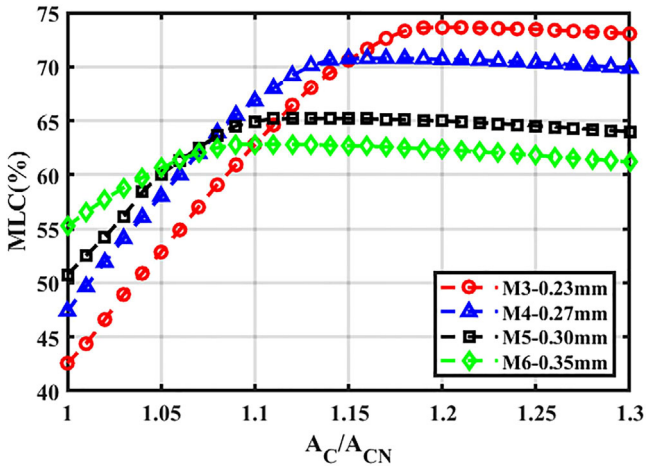

FIGURE 15 Variation of MLC with increment of core cross-sectional area for different core materials under 10 V/km DC bias

having higher permeability or lower reluctance draws higher excitation current. However, this is not the case for unsaturated transformers.

With the increment of the core cross-sectional area, the variation of MLC values of the transformer for the same core materials and DC bias condition is presented in Figure 15.

It is observed from Figure 15 that for considered four core materials, with increment of A_C/A_{CN}, at the first, the MLC ratio increases, reaches a highest value at the A_C/A_{CN} values in which saturation is eliminated and then decreases. Under saturation conditions, at the original cross-sectional area value ($A_C/A_{CN} = 1$), the MLC values are about 43%, 47%, 50%, and 55% for M3-0.23 mm, M4-0.27 mm, M5-0.30 mm, and M6-0.35 mm, respectively. In addition to that, the highest MLC values are about 74%, 70%, 65%, and 63% for M3-0.23 mm, M4-0.27 mm, M5-0.30 mm, and M6-0.35 mm, respectively.

4 | CONCLUSIONS

First of all, it is intended to investigate the effects of DC bias on performances of three-phase five-leg transformers by developing a computational efficient reluctance-based model. Current harmonic pollution, reactive power demand, DC, and frequency-dependent losses and maximum loading capability (MLC) are considered performance parameters. Here, it should be noted that the developed model can be used for the analysis of the transformer dedicated to supply non-linear loads [30–32].

Unlike the reluctance-based models previously proposed in the literature, it takes into account the frequency-dependent nature of the winding resistances. Accordingly, the developed model is validated with comparing 2D FEM model simulated in ANSYS Maxwell software under sinusoidal and DC-biased voltages.

And then, by using the suggested model, it is seen from the analysis performed for different DC-biased voltage conditions at no-load condition that the DC bias leads to saturation and increase in losses, reactive power demand, and excitation current's distortion for the studied transformer. Besides, by comparing the analysis results obtained in this study and the results previously presented in [7], it can be mentioned that the three-phase five-leg transformer is much more immune to the DC-biased voltages when compared with single-phase shell-type transformer.

Finally, under DC-biased voltage conditions, the magnetic material selection and legs cross section sizing on MLC are investigated. For the analysis, the considered core materials are in order of magnetic permeability from largest to smallest as follows M3-0.23 mm, M4-0.27 mm, M5-0.30 mm, and M6-0.35 mm. In the analysis, the cross-sectional areas of the yokes and outer legs of the transformer are varied. The cross-sectional areas are not changed on the main legs where the windings are located. This is because the cross-section increase in the main legs changes the size and impedance of the windings. The main findings concluded from the analysis can be arranged as follows:

- Under saturation conditions, the transformers, which have the core material with higher permeability or lower reluctance, draw higher excitation current, and have lower MLC ratio when compared with ones having the core material with lower permeability or higher reluctance.
- However, for unsaturated transformers, which work under DC bias, the case is the opposite of that in saturation conditions.
- Transformers with high permeable core material need more increment of cross-sectional area to escape the saturation related to DC bias when compared with ones with low permeable core material.
- For DC bias conditions, the effect of cross-sectional area on the MLC ratio is much larger for the transformer with high permeable magnetic core material with regards to ones with low permeable magnetic core material.

In future studies, for DC bias conditions, the authors will plan to study optimal design of transformers using developed model in this study. Three windings case of the transformer will also be studied in the future works.

ACKNOWLEDGEMENT

The design data and measurement test results, which are needed for the transformer modelling, were supplied with BEST Transformers Co.

CONFLICT OF INTEREST

The authors declare no conflict of interest.

DATA AVAILABILITY STATEMENT

The data that support the findings of this study are available from the corresponding author upon reasonable request.

ORCID

Sevket Canturk https://orcid.org/0000-0001-5439-5405
Murat Erhan Balci https://orcid.org/0000-0001-8418-8917
Mehmet Hakan Hocaoglu https://orcid.org/0000-0001-6528-3812

REFERENCES

1. Li, J., Li, J.: Core form transformer topological duality based transient model validation for exciting current calculation within DC bias. IET Gener. Transm. Distrib. 14(15), 3099–3107 (2020)
2. Price, P.R.: Geomagnetically induced current effects on transformers. IEEE Trans. Power Del. 17(4), 1002–1008 (2002)
3. Zhang, B., Zeng, R., He, J., Zhao, J., Li, X., Wang, Q., Cui, X.: Numerical analysis of potential distribution between ground electrodes of HVDC system considering the effect of deep earth layers. IET Gener. Transm. Distrib. 2(2), 185–191 (2008)
4. Zhang, B., Zhao, J., Zeng, R., He, J.: Numerical analysis of DC current distribution in AC power system near HVDC system. IEEE Trans. Power Del. 23(2), 960–965 (2008)
5. Rahman, M.A.,Islam, M.R.,Rahman, A.M.M.U., Muttaqi, K.M., Sutanto, D.: Investigation of the effects of DC current injected by transformer-less PV inverters on distribution transformers. IEEE Trans. Appl. Supercond. 29(2), 1–4 (2019)
6. Zhang, B., Cui, X., Zeng, R., He, J.: Calculation of DC current distribution in AC power system near HVDC system by using moment method coupled to circuit equations. IEEE Trans. Magn. 42(4), 703–706 (2006)
7. Canturk, S., Balci, M.E., Hocaoglu, M.H., Koseoglu, A.K.: Investigation of the effects of DC Bias on single-phase shell type transformers using frequency-dependent reluctance based model. IEEE Trans. Magn. 57(9), 1–9 (2021)
8. Hussein, A.A., Ali, M.H.: Fuzzy logic controlled variable resistor for suppressing GIC in transformers. IET Gener. Transm. Distrib. 11(6), 1494–1501 (2017)
9. Harrison, C.W., Anderson, P.I.: Characterization of grain-oriented electrical steels under high DC biased conditions. IEEE Trans. Magn. 52(5), 1–4 (2016)
10. Bíró, O., Buchgraber, G., Leber, G., Preis, K.: Prediction of magnetizing current wave-forms in a three-phase power transformer under DC bias. IEEE Trans. Magn. 44(6), 1554–1557 (2008)
11. Yang, P.H., Li, Y., Liu, L.G., Dong, X.L., Zhang, J.J.: Optimal placement of grounding small resistance in neutral point for restraining voltage fluctuation in power grid caused by geomagnetic storm. IET Gener. Transm. Distrib. 13(8), 1456–1465 (2019)
12. Girgis, R.S., Ko, C.D.: Calculation techniques and results of effects of GIC currents as applied to large power transformers. IEEE Trans. Power Deliv. 7(2), 699–705 (1992)
13. Girgis, R., Vedante, K.: Methodology for evaluating the impact of GIC and GIC capability of power transformer designs. In: 2013 IEEE PES T&D Conf. Exp., Vancouver, BC, Canada, (2013)
14. Wang, W., Nysveen, A., Magnusson, N.: Power losses in the three-phase three-limb transformer due to common and differential mode of dc-bias. IET Gener. Transm. Distrib. 15(1), 1488–1498 (2021)
15. Zhang, X., Liu, X., Guo, F., Xiao, G., Wang, P.: Calculation of DC bias reactive power loss of converter transformer via finite element analysis. IEEE Trans. Power Deliv. 36(3), 751–759 (2021)
16. Masoum, M.A.S., Moses, P.S.: Impact of balanced and unbalanced direct current bias on harmonic distortion generated by asymmetric three-phase three-leg transformers. IET Electr. Power Appl. 4(7), 507–515 (2010)
17. Moses, P.S., Masoum, M.A.S.: Three-phase asymmetric transformer aging considering voltage-current harmonic interactions, unbalanced nonlinear loading, magnetic couplings, and hysteresis. IEEE Trans. Energy Conv. 27(2), 318–327 (2012)
18. Aboura, F., Touhami, O.: Effect of the GICs on magnetic saturation of asymmetric three-phase transformer. IET Electr. Power Appl. 11(7), 1306–1314 (2017)
19. AmoiralisS, E.I., Tsili, M.A., Kladas, A.G.: Transformer design and optimization: A literature survey. IEEE Trans. Power Deliv. 24(4), 1999–2024 (2009).
20. Wang, S., Li, L., Zhao, X., Xie, Y., Cai, L.: Asymmetrical DC bias analysis of the no-load series transformer by using the TPFEM. IET Electr. Power Appl. 11(2), 169–177 (2017).
21. Zhang, B., et al. Effect of geomagnetically induced current on the loss of transformer tank. IET Electr. Power Appl. 4(5), 373–379 (2010).
22. Mikhak-Beyranvand, M., Faiz, J., Rezaeealam, B.: Thermal analysis and derating of a power transformer with harmonic loads. IET Gener. Transm. Distrib. 14(7), 1233–1241 (2020).
23. IEEE standard test code for liquid-immersed distribution, power, and regulating transformers. IEEE C57.12.90 (2015)
24. IEEE recommended practice for establishing liquid immersed and dry-type power and distribution transformer capability when supplying nonsinusoidal load currents. IEEE C57.110 (2018)
25. Mathworks,"Simulinkdocumentation", https://www.mathworks.com/help/physmod/sps/examples/three-phase-core-type-transformer.html, last accessed July 2021
26. Hussein, A.A., Ali, M.H.: Suppression of geomagnetic induced current using controlled ground resistance of transformer. Elect. Power Syst. Research 140(1), 9–19 (2016)
27. Boteler, D.H., Pirjola, R.J.: Modeling geomagnetically induced currents. Space Weather 15(1), 258–276 (2017)
28. Balci, M.E., Emanuel, A.E.: Apparent power definitions: A comparison study. Int. Rev. Elect. Eng. 6(6), 2714–2722 (2011)
29. The User's Guide of ANSYS Maxwell Release 18 Electromagnetics Simulation Software. (2020)
30. Arslan, E., Sakar, S., Balci, M.E.: On the no-load loss of power transformers under voltages with sub-harmonics. In: 2014 IEEE International Energy Conference (ENERGYCON), Cavtat, Croatia, 228–233 (2014)
31. Balci, M.E.: Optimal C-type filter design to maximize transformer's loading capability under non-sinusoidal conditions, electric power components and systems. Elect. Power Components Syst. 42(14), 1565–1575 (2014)
32. Arslan, E., Balci, M.E., Hocaoglu, M.H.: An analysis into the effect of voltage harmonics on the maximum loading capability of transformers. In: 2014 16th International Conference on Harmonics and Quality of Power (ICHQP), Bucharest, Romania, 616–620 (2014)

How to cite this article: Canturk, S., Balci, M.E., Hocaoglu, M.H., Koseoglu, A.K.: Performance analysis of three-phase five-leg transformers under DC bias using a new frequency-dependent reluctance-based model. IET Gener. Transm. Distrib. 16, 2455–2465 (2022). https://doi.org/10.1049/gtd2.12465

APPENDIX

The studied transformer's properties are given in Table A1.

The studied transformer's construction is drawn in Figure A1.

The transmission line parameters are presented in Table A2.

TABLE A1 Properties of the studied transformer

Parameters	Value
Winding structure	YnYn
Primary winding R_{dc} (Ω)	0.7322
Primary winding L (mH)	67.4
Secondary winding R_{DC} (Ω)	0.0597
Secondary winding L (mH)	10.15
Load losses (KW)	260
No-load losses (KW)	48

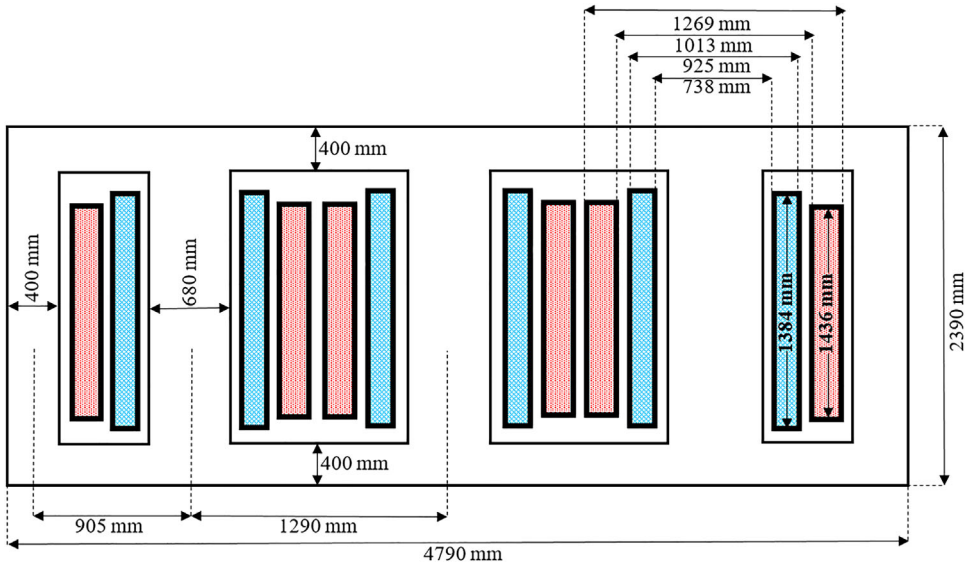

FIGURE A1 The drawing of transformer construction

TABLE A2 Transmission line parameters in the test system

Parameters	Value
Resistance	0.003068 pu
Inductive reactance	0.014399 pu
Admittance	0.006167 pu

For the simulated core materials, the *B*–*H* and *P*–*B* curves data are presented in Table A3.

TABLE A3 *B*–*H* and *P*–*B* data of the simulated core materials

	M3-0.23 mm		M4-0.27 mm		M5-0.30 mm		M6-0.35 mm	
B (T)	***P* (W/kg)**	***H* (A/m)**	***P* (W/kg)**	***H* (A/m)**	***P* (W/kg)**	***H* (A/m)**	***P* (W/kg)**	***H* (A/m)**
0.2	0.0128	6.8	0.017	5.3	0.0165	4.9	0.0203	4.2
0.4	0.049	10.2	0.0623	7.9	0.0623	7.1	0.0745	6.1
0.6	0.108	12.1	0.133	10.3	0.135	9.2	0.159	9.2
0.8	0.188	14.9	0.228	12.8	0.235	11.5	0.274	11.5
1.0	0.290	17.7	0.349	16.0	0.364	14.3	0.420	15.2
1.2	0.417	21.4	0.498	19.3	0.523	18.9	0.601	18.4
1.4	0.579	32.9	0.689	28.7	0.725	27.8	0.826	26.3
1.6	0.824	70.2	0.966	67.8	1.01	66.5	1.13	65.5
1.8	1.39	478.8	1.55	467.8	1.56	459.7	1.69	452.7